Submitted to JAMES

Community Earth System Model version 2 (CESM2) Special Collection

Seasonal mean monsoon simulations in CESM2

Gerald A. Meehl[1], Christine Shields[1], Julie M. Arblaster[1,2], H. Annamalai[3], and Richard Neale[1]

1. National Center for Atmospheric Research, Boulder, CO, ORCID: 0000-0002-8760-9534
2. ARC Centre of Excellence for Climate Extremes, Monash University, Melbourne, Australia
3. IPRC/Department of Oceanography, University of Hawaii at Manoa, HI

November 26, 2019

Key Points:

- Community Earth System Model version 2 (CESM2) is compared to observations and the previous generation CESM1 for seasonal mean simulations of precipitation and surface winds for the south Asian and Australian monsoons, the West African monsoon, the North American monsoon, and the South American monsoon.
- Notable improvements are seen in CESM2 compared to CESM1 for most monsoon regimes.
- The seasonal timing of the south Asian monsoon, monsoon-ENSO connections, and monsoon intraseasonal variability all are improved compared to CESM1 and mostly compare favorably with observations

Keywords: Global coupled Earth system modeling; Asian-Australian monsoon; West African monsoon; North American monsoon; South American monsoon

Plain Language Summary

A survey of seasonal mean simulations of regional precipitation and 850hPa winds is presented for the Community Earth System Model version 2 (CESM2) compared to observations and the previous generation CESM1 for the south Asian and Australian monsoons, the West African monsoon, the North American monsoon, and the South American monsoon. There are mostly improvements in the distribution of seasonal mean rainfall in CESM2 compared to CESM1 in the monsoon regimes. The seasonal timing of the south Asian monsoon, monsoon-ENSO connections, and monsoon intraseasonal variability all are improved compared to CESM1 and mostly compare favorably with observations.

Abstract

A survey of seasonal mean regional precipitation and 850hPa winds for various monsoon regimes is presented for the Community Earth System Model version 2 (CESM2) compared to observations and the previous generation CESM1. These improvements in CESM2 include, for the south Asian monsoon, a reduction of excessive precipitation in the western Indian Ocean and an increase of precipitation in the eastern Bay of Bengal and land areas of Vietnam, Cambodia and Laos. The seasonal timing of the south Asian monsoon, monsoon-ENSO connections, and monsoon intraseasonal variability all are improved compared to CESM1. For the Australian monsoon, deficient precipitation over the Maritime Continent has been improved in CESM2 with increases of precipitation over the large tropical islands of Borneo, Celebes, and Papua New Guinea, and decreases over southwestern Australia. In the West African monsoon, MJ seasonal rainfall occurs more preferentially over the African coast in CESM2 as in observations, and excessive rainfall over the Ethiopian region is reduced in CESM2. In JAS in the West African monsoon, the CESM1 error of deficient precipitation over equatorial Africa has been lessened in CESM2, and there are increases in precipitation over the Guinean coast. In the South American monsoon, DJFM precipitation in CESM2 is improved with more extensive precipitation over central and western Brazil, though there is still excessive precipitation over eastern Brazil compared to observations. CESM2 simulates a reduction of excessive precipitation seen in CESM1 over coastal Mexico extending up into the U.S. Great Plains in the North American monsoon.

1. Introduction

As part of the ongoing model development and improvement process for the Community Earth System Model (CESM), the monsoon simulations in successive generations of models have been evaluated (Meehl et al., 2006; Meehl et al., 2012; Cook et al., 2012; Shields et al., 2016). Though there has been a steady improvement in many aspects of the monsoon simulations, a number of systematic errors remain to be addressed. The purpose of this paper is to describe the seasonal precipitation and low level wind features of the monsoon simulations in major monsoon regimes around the world in the latest version of CESM, the CESM2 (Danabasoglu et al., 2019) in comparison to the previous generation of model, the CESM1, and to observations. The fidelity of subseasonal variability related to the Asian-Australian monsoon regimes also will be examined. In doing so, we will link the limitations in seasonal mean climatology (basic state) to modeled variability aspects.

2. Models and observations

The components and coupled simulations of CESM1 were described by Hurrell et al. (2013), for CESM1.1 by Kay et al., (2015), and for CESM1.3 by Meehl et al., (2019). The atmospheric model in CESM1 had a nominal 1 degree latitude-longitude resolution, as did the ocean with enhanced resolution in the latter near the equatorial waveguide. The CESM2 has had a number of improvements and modifications from the versions of CESM1 (Danabasoglu et al 2019). In the atmosphere, the resolution is the same; however, a number of features that directly affect monsoon regimes involving the boundary layer, convection schemes, and precipitation processes have been improved. The separate representations of the boundary layer, shallow convection

and large-scale condensation (e.g. the boundary layer in the University of Washington, UW, scheme and Park scheme for shallow convection and macrophysics in CESM1) have been replaced by the Clouds Unified By Binormals (CLUBB, Golaz et al., 2002). CLUBB is a high order turbulence closure scheme, and uses simple PDFs to describe the sub-grid scale distributions of key humidity, saturation, temperature and vertical velocity quantities. The previous version of the Morrison Getteleman (MG1) microphysics scheme in CESM1 has been updated to MG2 in CESM2 that now predicts rather than diagnoses precipitating hydrometeors (Gettelman and Morrison, 2015). Direct modifications to the Zhang McFarlane deep convection scheme (Neale et al., 2008; Zhang and McFarlane, 1995) act to further increase humidity sensitivity and the near-surface stress scheme of Beljaars et al., (2004) acts to reduce excessive drag seen in CESM1. The final major change is to advance the modal aerosol scheme from 3 to 4 modes (MAM4, Liu et al., 2014) which includes an improved aging process for black carbon.

The ocean model in CESM2 is a version of PoP used in CESM1 but with many improvements to the physics (Danabasoglu et al., 2019). It has a nominal 1 degree horizontal resolution and enhanced resolution in the equatorial tropics, and 60 levels in the vertical with ocean biogeochemistry. Other features of CESM2 involving land and sea ice are described in detail by Danabasoglu et al., (2019).

Observations used here include TRMM/ERA-I gridded precipitation (Huffman et al., 2007), and ERA-I 850 hPa winds and sea surface temperatures (SSTs) (Dee et al., 2014)

3. The South Asian monsoon

Seasonal mean precipitation (June-July-August-September, JJAS) for CESM1, CESM2, observations (TRMM/ERA-1), the difference CESM2 minus CESM1, and respective differences of the model simulations from observations are shown in Fig. 1. A persistent systematic error that has been present in previous versions of CESM and in other earth system models as well (e.g. Sperber et al. 2013; Annamalai et al., 2017) is precipitation maxima that extend too far west in the western Indian Ocean, as seen in CESM1 (Fig. 1b) compared to observations (Fig. 1c, f). This systematic error has been reduced somewhat in the CESM2. Tracking the position of the 6 mm day^{-1} contour in observations near the equator, it lies at about 60^oE (Fig. 1c). In CESM1 it was around 70^oE (Fig. 1b), and in CESM2 it is farther east and closer to the observed location of about 60^oE (Fig. 1a). This movement of the western Indian Ocean precipitation maxima to the east in CESM2 in closer agreement with observations shows up as large negative differences in Fig. 1d of about -6 mm day^{-1}, with the large significant positive precipitation anomaly of 6mm day^{-1} in CESM1 compared to observations in the western Indian Ocean (Fig. 1f) reduced by about a third to roughly +2 mm day^{-1} in CESM2 (Fig. 1e) thus signalling improvement of this aspect of the seasonal monsoon pattern. However, the precipitation maximum near 5^oS seen in observations (Fig. 1c) with overly strong amplitude in CESM1 (Fig. 1b,f) has shrunk in CESM2 (Fig. 1a) with consequent significant negative precipitation deficits of about -5 mm day^{-1} near 5^oS (Fig. 1e). Therefore, some improvement in the westward extent of the precipitation maxima in the western Indian Ocean in CESM2 is accompanied by a reduction of the precipitation maximum at 5^oS.

Another flaw in the seasonal mean precipitation pattern in CESM1 was the virtual absence of the precipitation maximum in the eastern Bay of Bengal and the coasts of Myanmar and Thailand, with hardly any rainfall occurring over land areas of Vietnam, Cambodia and Laos (comparing CESM1 in Fib. 1b to observations in Fig. 1c). Consequently, there are significant negative precipitation differences for CESM1 minus observations of around -6 mm day^{-1} in those regions (Fig. 1f). However, CESM2 is considerably improved in these aspects with a quite strong precipitation maximum in that region (Fig. 1a) compared to observations (Fig. 1c), and represented by large significant positive precipitation differences of up to +6 mm day^{-1} in the western Bay of Bengal and over Indochina for CESM2 minus CESM1 (Fig. 1d). The increase of precipitation over land in CESM2, in closer agreement with observations here and in other monsoon regimes, is likely related to a response to the MG2 rain production (prognostic) versus MG1 (diagnostic). In terms of the magnitude it seems the increased humidity sensitivity in the deep convection is partly responsible, in addition to CLUBB in CESM2 versus UW in CESM1, which also smooths out the precipitation in the Bay of Bengal (UW). Even with these improvements in CESM2, there is still deficient rainfall of around -3 mm day^{-1} over northern India and the Bay of Bengal compared to observations (Fig. 1e).

Another systematic error present in CESM1 that has been improved in CESM2 is that monsoon precipitation in CESM1 that extended too far to the northwest over Pakistan now is more contained to the southeast in closer agreement with observations (Fig. 1a,b,c). This is evidenced by significant negative precipitation differences over northwest Pakistan of about -3 mm day^{-1} for CESM2 minus CESM1 (Fig. 1d), and negative anomalies of less than ~ -1 mm day^{-1} for CESM2 minus observations (Fig. 1e).

In summary, compared to CESM1, in CESM2 we note a redistribution of seasonal mean precipitation, improving it in some regions (western Indian Ocean, land areas of southeast Asia) while deteriorating in other regions (near 5^{o}S in the Indian Ocean). This is very typical of state-of-the-art coupled models, and clearly implicates the interactive and intertwined processes that make up the regional monsoon precipitation climatology over South Asia (e.g., Annamalai et al. 2019).

The major features of the 850 hPa wind field are captured relatively well in CESM2 as they were in CESM1 compared to observations, with strong cross-equatorial flow in the western Indian Ocean, and westerlies carrying right across the Indian subcontinent and on to Indochina (Fig. 1a,b,c). Winds over the Bay of Bengal in CESM2 are stronger by about 20% compared to CESM1 and in closer agreement with observations in association with the increased precipitation in the eastern Bay of Bengal and Indochina. Simulating the wind patterns has higher skill due to the fact the wind response depends on the integrated diabatic heating and not on the regional details of the simulated precipitation (e.g., Sperber et al. 2013).

The timing of the seasonal monsoon maximum can be as important as the amount of precipitation itself. Fig 2 shows the monthly timing of the climatological precipitation maximum over the region. On the whole the observed timing peak occurs in July over the Indian subcontinent (a few regions have wintertime peaks associated with the northeast winter monsoon) (Fig. 2a) . In CESM1 the peak occurs more during August, even into the Bay of Bengal where the observed peak is much earlier in June (Fig. 2c). CESM2 broadly improves on

this with the peak now occurring during July (Fig. 2b). In observations, to the east the observed peak occurs progressively (from June over Bay of Bengal to September over South China Sea) illustrating the eastward extension of the mean monsoon precipitation. In the model, this feature is reasonably simulated despite a stronger wet bias over the plains of Indo-China in CESM2 (Fig. 1).

4. **Monsoon-ENSO connections in CESM2**

An important component of any model development is to assess if the model realistically captures the impact of ENSO on the monsoon precipitation and circulation at interannual timescales since extreme droughts and flood conditions over South Asia are determined by ENSO characteristics (e.g., Sikka 1980; Shukla and Mooley 1983; Pillai and Annamalai 2012). A simple metric for assessing ENSO-monsoon association is to calculate the simultaneous correlation of area-average JJAS all-India rainfall (AIR, land points averaged over 7^{o}N–30^{o}N, 65^{o}E–95^{o}E) with surface temperature for CESM2 and observations (AIR index computed from observed precipitation over India, Fig. 3) for the 1950-2010 period. The CESM2 captures the observed opposition of sign between monsoon rainfall and eastern tropical Pacific SSTs, with above normal monsoon rainfall associated with below normal eastern tropical Pacific SSTs and vice-versa. Above normal monsoon rainfall also is associated with below normal surface temperatures over the Indian monsoon land regions and in the western Indian Ocean and Arabian Sea due to enhanced cloudiness and rainfall, and stronger winds that produce cooler SSTs, respectively. As in previous generations of CESM (e.g. Meehl et al., 2012), the negative correlations in the equatorial eastern Pacific reach too far westward, with the zero line extending nearly to 130^{o}E compared to observations farther east at 160^{o}E. The model correlations are of

greater magnitude with larger areas of statistical significance compared to the observations in association with Nino3.4 standard deviations being about 30% stronger than observations in CESM2 (Capotondi et al., 2019). For example, the extent of the -0.5 correlation in the equatorial Pacific in CESM2 extends from about 165^{o}E to 100^{o}W (Fig. 3a), while in the observations it ranges from about 170^{o}W to 120^{o}W (Fig. 3b). However, maximum values of the negative correlations in the eastern equatorial Pacific are roughly comparable, with values between -0.5 and -0.6 in both the CESM2 and observations.

The strength of the negative correlation between monsoon rainfall and tropical Pacific SSTs relates to the dynamics of the large-scale east-west (Walker) circulation between the Pacific and Indian sectors. Thus, during a composite observed El Nino event, maximum SSTs of nearly 30^{o}C set up near the Dateline during November and December of the year of onset of the event (year 0, Fig. 4c) associated with precipitation values of 10 mm day^{-1} extending from the Dateline to about 150W during December of year 0 to February of year+1 (Fig. 4c). These precipitation maxima are preceded by comparable precipitation values near 150^{o}E during February and May of year 0. For CESM2, somewhat larger SST values of about 31oC set up at about the same time but are about 10 degrees of longitude farther west (Fig. 4a) as those seen in the observations (Fig. 4c), with correspondingly larger values of precipitation up to 18 mm day^{-1}, but with roughly the same seasonal timing and westward shift in location as in the observations. This is an improvement from previous model versions (Meehl et al., 2012) where the model simulated the maximum SST and precipitation values even farther west. Thus, with the improved position and seasonal timing of ENSO SST and precipitation values, the anomalous Walker Circulation

229 should set up in a comparable location and provide similar magnitude negative correlations
230 between Indian monsoon rainfall as represented by the observed AIR index.
231
232 In addition to the well-known relationship between above normal AIR and below normal eastern
233 tropical Pacific SSTs, the magnitude of this correlation is known to fluctuate on interannual to
234 decadal timescales (e.g., Parthasarathy et al. 1991; Meehl et al., 2012), perhaps associated with
235 decadal modulation of ENSO characteristics (e.g., Annamalai et al. 2007) or aspects of tropical
236 Indian Ocean variability (e.g., Ashok et al. 2001). To examine this relationship as a function of
237 time, a running 13 year correlation is shown in Fig. 5 between the JJAS AIR and the JJAS
238 Nino3.4 SSTs. CESM2 better captures the strength of this observed correlation compared to
239 previous model versions shown by Meehl et al. (2012). Correlations in the historical simulations
240 in CESM2 range from about -0.9 to -0.5 with two occurrences of near zero correlation and one
241 occurrence of a positive correlation of about +0.2 (Fig. 5b). This compares favorably with the
242 observations (Fig. 5a) with a similar range and one occurrence of a positive correlation of around
243 +0.2. There were smaller negative correlations in CCSM4 of -0.7 to -0.2 with numerous
244 occasions of positive correlations nearing +0.2 in the earlier model (Meehl et al., 2012). These
245 characteristics were also present in CESM1.
246
247 Additionally, the magnitude of these correlations could be affected by the amplitude of ENSO
248 and position of maximum SST and precipitation during ENSO events. As noted above, though
249 the maximum SST and precipitation values are shifted a bit west during ENSO events in
250 CESM2, these are better simulated than in CESM1 and CCSM4. The larger values in CESM2
251 compared to observations provide larger forcing of the large-scale divergent circulation and

reinforce a strong monsoon-ENSO connection. This quantity is much improved in CESM2 compared to earlier versions such as CESM1, though there could be compensating errors that produce this improvement (Simpson et al., 2019). With regards to amplitude, CESM2 ENSO is about 30% larger than observed but closer to observations than in CCSM4 or CESM1, with comparable frequency compared to observations (Deser et al., 2012; Capotondi et al 2019).

In summary, improvements in position of maximum SST and precipitation during ENSO events compared to earlier model versions, even with somewhat of a westward shift, contribute to an improved upper level divergent circulation and the magnitude of the monsoon-ENSO negative correlation that is close to observations.

5. **Australian monsoon**

Two of the major flaws in the simulation of seasonal (December-January-February, DJF) precipitation in the Australian monsoon in CESM1 were the deficient rainfall over the maritime continent, and excessive precipitation too far to the southwest over Australia (Fig. 6b compared to observations in Fig. 6c). Both of these deficiencies have been improved in CESM2 (Fig. 6a). There are significant increases of precipitation particularly over the large tropical islands of Borneo, Celebes, and Papua New Guinea of around 5 mm day^{-1}, and decreases of about that same magnitude over southwestern Australia (Fig. 6d). With these improvements has come a decrease in the CESM2 precipitation maxima over northern Australia and the Gulf of Carpentaria with CESM2 maxima in those regions about 20% less than observations (comparing CESM2 in Fig. 6a to observations in Fig. 6c). The improvements in CESM2 compared to

CESM1 related to observations produce lower amplitude differences from observations over most of the Australian monsoon domain (comparing Figs. 6e,f).

In association with these improvements in the regional precipitation distribution, the low-level winds also have improved in CESM2 compared to CESM1, particularly over Australia where there are now well-defined easterlies over most of the country (Fig. 6a) as in observations (Fig. 6c) compared to northeasterlies in CESM1 (Fig. 6b).

6. Factors affecting the Asian-Australian monsoon simulations

It has been speculated that the systematic error for the South Asian monsoon of too much precipitation too far west in the western Indian Ocean could be affected by an overly strong cold tongue in the Pacific and deficient precipitation over the Maritime Continent (e.g. Meehl et al 2012) or an overly strong Bjerknes' feedback along the equatorial Indian Ocean (Annamalai et al. 2017) or limitations in representing regional air-sea interactions off Somali-Oman coasts and associated atmospheric boundary-layer processes (Hanf and Annamalai 2019). Fig. 7 shows annual mean SST and surface wind stress for observations, CESM2, CESM1, and the difference, CESM2 minus CESM1. In CESM2 (Fig. 7b), SSTs in the Western Pacific Warm Pool exceed 30oC and are roughly 1-2oC warmer than in CESM1 (Fig. 7c) and about 1oC warmer than observations (Fig. 7a). This is consistent with about the same increase in magnitude of SST near the Dateline in ENSO events (Fig. 4). The excessively low SSTs in the eastern Pacific cold tongue in CESM1 (Fig. 7c) are now closer to observations (Fig. 7a) in CESM2 (Fig. 7b). Consequently there are weaker trade winds in the northeastern tropical Pacific in CESM2 compared to CESM1 (southwesterly anomalies in Fig. 7d). The reduced double ITCZ in CESM2

(Danabasoglu et al, 2019) is associated with stronger southeast trades in the southeast tropical Pacific (southeasterly anomalies in Fig. 7d) and SSTs in the southeastern tropical Pacific that are cooler in CESM2 compared to CESM1 by about 1oC (Fig. 7d). The warmer than observed SSTs over the western Pacific warm pool in CESM2 (Fig. 7b) act to increase precipitation over the Maritime Continent in CESM2 and draw the center of gravity for monsoon precipitation farther east and closer to observations (comparing Figs. 1 and 6).

7. Intraseasonal variability in the Asian-Australian monsoon

a. *Northward propagating intraseasonal oscillations in the South Asian monsoon*

Figure 8 for JJAS shows a composite analysis of the coherent intraseasonal propagating events that originate over the tropical central-eastern Indian Ocean east Pacific during the monsoon and propagate northwards through the Bay of Bengal and extend over land. Such a northward propagating precipitating feature is called either the Intraseasonal Oscillation (ISO, e.g. Karmakar and Krishnamurti, 2019), the Monsoon Intraseasonal Oscillation (MISO, e.g. Suhas et al., 2012), or the Boreal Summer Intraseasonal Oscillation (BSISO, Yusanari, 1979). All refer to the same phenomenon (we will use BSISO here) that is the dominant subseasonal mode of the Indian monsoon and lies at the center of the active-break monsoon cycles of the region (e.g., Sikka and Gadgil 1980). Compared to its northern winter-time counterpart, the Madden Julian Oscillation (MJO, discussed below) in which the convective anomalies are predominant along the equatorial latitudes and have a large influence on Australian monsoon intraseasonal variability (e.g., Madden and Julian 1994; Hung et al. 2013), the BSISO has eastward and poleward propagating components over the tropical Indo-West Pacific regions (e.g., Lau and Lau 1986; Annamalai and Sperber 2005). These northward-propagating disturbances characterized by

the BSISO remain a simulation challenge for climate models (Sperber and Annamalai 2014; Neena et al., 2016; Sabeerai et al., 2013), and yet they are crucial for monsoon prediction within a season (Goswami and Xavier, 2003). CCSM4 (Meehl et al., 2012) and CESM1 (Fig. 8c) were similar in that both model versions underestimated both the coherence and northward propagation characteristics of the BSISO. Although the surface zonal winds and precipitation signals are somewhat in quadrature just north of the equator and at around 20$_o$N, there is no propagation connection between the two in CESM1 (Fig. 8c). CESM2 represents a significant improvement, exhibiting coherent northward propagating events of precipitation and surface winds that are in quadrature (Fig. 8b compared to observations in Fig. 8a). One degradation, however, is a lack of northward connection from south of the Indian Ocean compared observations. It is possible that limitations in simulating this aspect of BSISO relate to the model's fidelity in representing the basic state (Sperber and Annamalai, 2008). They suggested that there should be a minimum intensity of precipitation over the equatorial Indian Ocean to force Rossby waves that then appear as part of a poleward migration. There is a clear connection to improvements in BSISO in CESM2 compared to CESM1 from examination of the regional improvements in mean precipitation distribution described earlier (Fig. 1). For example, there are precipitation increases in the Bay of Bengal (an improvement) but decreases south of the equator (a degradation) between CESM2 and CESM1. The former likely contribute to the overall improvement in BSISO in CESM2, while the latter could be affecting the lack of connection from the south Indian Ocean.

b. Intraseasonal variability associated with the MJO in the Australian monsoon in DJF

The Australian monsoon variability seems to also benefit from improvement in the intraseasonal oscillations, in this case the MJO. The Indo-Pacific region has a very consistent composite eastward propagating signal, with precipitation surface quadrature coherence that extends through the Australian Monsoon region (Fig. 9b compared to 9a). In CESM1, any intraseasonal signal is confined entirely to the Indian ocean, with an erroneous westward propagation (Fig. 9c). Thus, the Australian Monsoon region in CESM1 is not subject to any appreciable variability associated with MJO events, but has a larger contribution from MJO variability in CESM2. In response to a number of parameterization changes (e.g., Bogenschutz et al., 2017) and because of a different response to the underlying SST distributions, CESM2 supports stronger and more regionally extensive MJO events that are now able to propagate out of the Indian Ocean and into the West Pacific. This, therefore, subjects the Maritime Continent and the Australian monsoon region to a much more realistic level of intraseasonal monsoon variability.

8. **West African Monsoon**

There are two distinct warm-season precipitation regimes over West Africa, namely, the May–June (MJ) period of strong Guinean coast rainfall and the July–September (JAS) period with rainfall in the Sahel (Cook et al., 2012), and we show both periods here.

There were several features of the MJ West African Monsoon simulation in CCSM4 that were viewed as deficient (Cook et al 2012). In general as shown for CESM1 in Fig. 10b compared to observations in Fig. 10c and the differences in Fig. 10f, there was too much rainfall over the Atlantic just south of the Guinean coast during MJ with differences exceeding +6 mm day^{-1}. Additionally, there was too much rainfall to the east over the Ethopian region, with positive differences approaching +3 mm day^{-1}. During the latter part of the monsoon season in JAS in

CESM1 (Fig. 11), there was generally deficient rainfall over the equatorial African regions with negative differences of around -3 mm day^{-1}. All of these features are generally improved in CESM2. The MJ rainfall occurs more preferentially over the African coast in CESM2 (Fig. 10a) compared to CESM1 (Fig. 10b) with increases of about +3 mm day^{-1} (Fig. 10d). Though CESM2 still simulates excessive precipitation to the south of the Guinean coast, the simulation errors are about half of what they were in CESM1 (Figs. 10e and f). The surface wind stress simulation is improved in CESM2 compared to CESM1 with the southeast trades shifting to near the equator where they were near 5^{o}S in CESM1 (comparing Figs. 10a,b). However, the CESM2 trades are still about 3 degrees of latitude south of where they are located in the observations at this time of year (Fig. 10c). Additionally, rainfall over the Ethiopian region to the east is closer to observations (Fig. 10c) in CESM2 (Fig. 10a) compared to CESM1 (Fig. 10b). These differences amount to about -3 mm day^{-1} in that region (Fig. 10d) with CESM2 having anomalies less than about +1 mm day^{-1} there compared to observations (Fig. 10e).

With regards to the later part of the monsoon season (JAS, Fig.11), as noted above the main error in CESM1 was that precipitation totals over equatorial Africa were too small (Fig. 11b,f). This error has been lessened in CESM2 with differences in precipitation there amounting to values greater than +3 mm day^{-1} or a nearly 50% increase in CESM2 compared to CESM1 (Fig. 11d). If anything, JAS seasonal precipitation totals are now about 15% too large in CESM2 compared to observations (Fig. 11e), but the spatial pattern captures the maxima near the Guinean coast and Nigeria seen in observations (Fig. 11c). However, CESM2 now simulates excessive precipitation over the Guinean coast with positive anomalies reaching nearly +2 mm day^{-1} with some small deficits in the Sahel (Fig. 11e). This precipitation feature is accompanied but surface

388 westerlies near 10$_o$N coming into West Africa from the Atlantic that are about 50% too strong in
389 CESM2 (Fig. 11a) as they were in CESM1 (Fig. 11b) compared to observations (Fig. 11c).
390
391 9. **South American monsoon**
392 One of the systematic errors in the South American monsoon seasonal precipitation pattern
393 (December-January-February-March, DJFM) in CESM1 was was deficient precipitation in the
394 central Amazon (Fig. 12b compared to 12a). That is, the precipitation maximum in CESM1 was
395 centered too far east over eastern Brazil (Fig. 12b) compared to observations where the
396 precipitation maximum is more over central and western Brazil (Fig. 12c). This produced
397 precipitation deficits in CESM1 compared to observations of nearly -5 mm day^{-1} in that region.
398 These errors were accompanied by surface easterlies that were too strong and extended too far
399 west between the equator and 10$_o$S. The DJFM seasonal precipitation and surface wind
400 simulation in CESM2 is improved in comparison to CESM1. There is more extensive
401 precipitation over central and western Brazil (comparing Figs. 12a and b) with positive
402 differences of 3-6 mm day^{-1} there (Fig. 12d). The surface easterlies start to recurve to the
403 northwest farther to the east in CESM2 (Fig. 12a) compared to CESM1 (Fig. 12b) which also is
404 in better agreement with observations (Fig. 12c). However, there is still excessive precipitation
405 in CESM2 over eastern Brazil compared to observations with anomalies of about +3 mm day^{-1}
406 (Fig. 12a compared to Fig. 12c, and differences from observations in Fig. 12e).
407
408 Another systematic error in CESM1 was excessive precipitation extending too far to the south
409 over the Andes in Bolivia and northern parts of Argentina and Chile (Fig. 12b) with differences
410 from observations of about +5 mm day^{-1} (Fig. 12b). Though this error has not totally gone away,

CESM2 shows improvements in this aspect, with reductions of precipitation in those regions compared to CESM1 of about -3 to -6 mm day^{-1} (Fig. 12d). This is accompanied by a reduction in magnitude of low level winds in CESM2 compared to CESM1 near the Andes with reduced implied surface convergence that would contribute to less precipitation there in CESM2.

10. **North American monsoon**

A striking systematic error of seasonal (June-July-August, JJA) precipitation in the North American monsoon in CESM1 compared to observations (Fig. 13b compared to 13c) was excessive precipitation over coastal southern Mexico extending up into the U.S. Great Plains, with significant differences from observations of the latter of about +3 mm day^{-1} (Fig. 13f). There has been a marked improvement in CESM2 compared to CESM1, with reduction of those precipitation errors of about -4 mm day^{-1} (Fig. 13d) to bring CESM2 in much better agreement with the observations (comparing Fig. 13a to 13c) where differences from observations in CESM2 in the Great Plains are near zero (Fig. 13f). This is accompanied by an improvement in the simulation of surface wind direction in CESM2 compared to CESM1, with CESM2 showing more of a southeast component to surface wind stress coming in off the Gulf of Mexico (Fig. 13a) in closer agreement with observations (Fig. 13c), while CESM1 has more of a southerly component (Fig. 13b).

One error that remains in CESM2 is that the coastal northwestern Mexico precipitation maximum is still somewhat weaker than observed and does not extend far enough northward. The CESM2 has negative precipitation anomalies compared to observations of up to about -3

433 mm day^{-1} along the northwestern Mexico coast comparable to what was simulated in CESM1
434 (Fig. 13f).
435
436 **11. Conclusions**
437 There have been a number of improvements to the various monsoon regimes around the world
438 from CESM1 to CESM2. These include:
439 1. Evidence of movement of the western Indian Ocean precipitation maximum to the east in
440 CESM2 in somewhat closer agreement with observations
441
442 2. Increase of the precipitation maxima in the eastern Bay of Bengal and the coasts of
443 Myanmar and Thailand, and land areas of Vietnam, Cambodia and Laos
444
445 3. Monsoon precipitation in CESM1 that extended too far to the northwest over Pakistan
446 now is more contained to the southeast in CESM2 in closer agreement with observations
447
448 4. The seasonal timing of the south Asian monsoon, monsoon-ENSO connections, and
449 monsoon intraseasonal variability all are improved compared to CESM1 and mostly
450 compare favorably with observations
451
452 5. Deficient precipitation over the Maritime Continent in CESM1 has been improved in
453 CESM2 with increases of precipitation over the large tropical islands of Borneo, Celebes,
454 and Papua New Guinea and decreases over southwestern Australia, all in closer
455 agreement with observations

6. In the West African monsoon, the MJ rainfall error in CESM1 of excessive rainfall over the Gulf of Guinea has been cut in half in CESM2, though rainfall there is still greater than observed; rainfall over the Ethiopian region to the east is reduced in CESM2 compared to CESM1 in closer agreement with observations

7. In JAS in the West African monsoon, the main error in CESM1 of deficient precipitation totals over equatorial Africa has been lessened in CESM2, though CESM2 now simulates excessive precipitation over the Guinean coast with some small deficits in the Sahel

8. The South American monsoon DJFM seasonal precipitation simulation in CESM2 is improved in comparison to CESM1 with regards to more extensive precipitation over central and western Brazil, though there is still excessive precipitation over eastern Brazil compared to observations

9. An error in CESM1 was excessive precipitation extending too far to the south over the Andes in Bolivia and northern parts of Argentina and Chile, but CESM2 shows improvements with reductions of precipitation in those regions in closer agreement with observations

10. A systematic error in the CESM1 North American monsoon simulation of excessive precipitation over coastal southern Mexico during JJA extending up into the U.S. Great Plains has been improved in CESM2, with reduction of those precipitation errors that

brings CESM2 into better agreement with the observations particularly over the Great Plains. Though somewhat improved from CESM1, in CESM2 coastal northwestern Mexico precipitation maximum is still weaker than observed and does not extend far enough northward.

Acknowledgments

The CESM project is supported primarily by the National Science Foundation (NSF). Computing and data storage resources, including the Cheyenne supercomputer, were used for the CESM simulations (doi:10.5065/D6RX99HX). Portions of this study were supported by the Regional and Global Model Analysis (RGMA) component of the Earth and Environmental System Modeling Program of the U.S. Department of Energy's Office of Biological & Environmental Research (BER) via National Science Foundation IA 1947282. This work also was supported by the National Center for Atmospheric Research, which is a major facility sponsored by the National Science Foundation (NSF) under Cooperative Agreement No. 1852977. H. Annamalai is supported by an NSF project under Grant 1460742.

Model and Data Availability

Previous and current CESM versions are freely available at www.cesm.ucar.edu:/models/cesm2/. The CESM solutions / datasets used in this study are also freely available from the Earth System Grid Federation (ESGF) at esgf-node.llnl.gov/search/cmip6 or from the NCAR Digital Asset Services Hub (DASH) at data.ucar.edu or from the links provided from the CESM web site at

www.cesm.ucar.edu. HADiSST data are available from: https://www.metoffice.gov.uk/hadobs/hadisst/.

GPCP precipitation data are available from: https://www.esrl.noaa.gov/psd/data/gridded/data.gpcp.html.

The All-India Rainfall is available from: https://data.gov.in/catalog/all-india-area-weighted-monthly-seasonal-and-annual-rainfall-mm?filters%5Bfield_catalog_reference%5D=85825&format=json&offset=0&limit=6&sort%5Bcreated%5D=desc.

The TRMM rainfall data are available from: https://pmm.nasa.gov/data-access/downloads/trmm and GPCP rainfall data from https://www.esrl.noaa.gov/psd/data/gridded/data.gpcp.html.

The ERA-I data are available from: https://www.ecmwf.int/en/forecasts/datasets/reanalysis-datasets/era-interim.

The Large and Yeager (2009) surface wind stress data are available from: https://climatedataguide.ucar.edu/climate-data/corev2-air-sea-surface-fluxes

References

Annamalai, H., et al. (2017). Systematic errors in South Asian Monsoon simulation: Importance of equatorial Indian Ocean processes. *J. Clim*., *30*, 8159--8178. DOI: 10.1175/JCLI-D-16-0573.1.

Annamalai, H., Hamilton, K., & and Sperber, K.R. (2007). South Asian Summer Monsoon and its relationship with ENSO in the IPCC AR4 simulations. *J. Clim.*, *20*, 1071-1092.

Annamalai, H., W. Boos, G. Martin, B. Mapes, Y. Ming, P. Mukhopadhyay, T.-Y. Koh, and S. Rao, 2019: CLIVAR-GEWEX Working Group on Asian-Australian Monsoons: Grand Challenges in Monsoon Modeling – Representation of Processes and Source of Model Errors. A book chapter for the IWM6 monograph on Monsoons (invited article – in press)

Beljaars, A. C. M., A. R. Brown, A..R., & Wood, N. (2004). A new parametrization of turbulent orographic form drag. *Quarterly Journal of the Royal Meteorological Society*, *130*, 1327–1347, doi:10.1256/qj.03.73.

Bogenschutz, P. A., Gettelman, A., Hannay, C., Larson, V.E., Neale, R.B., Craig, C., & Chen, C.-C. (2018). The Path to CAM6: Coupled Simulations with CAM5.4 and CAM5.5. *Geosci. Mod. Dev*., *11*, 235–255, doi:10.5194/gmd-2017-129.

Capotondi, A., et al. (2019). ENSO in CESM2. *JAMES*, submitted.

Cook, K.H., Meehl, G.A., & Arblaster, J.M. (2012). Monsoon regimes and processes in CCSM4. Part 2: The African and American monsoons. *J. Climate*, *25*, 2609—2621, doi: 10.1175/JCLI-D-11-00185.1.

Danabasoglu, G., et al. (2019). The Community Earth System Model version 2 (CESM2), *JAMES*, submitted.

Dee, D.P. et al. (2014). Toward a consistent reanalysis of the climate system. *Bull. Amer. Meteor. Soc.*, *95(8)*, 1235-1248.

Deser, C., et al. (2012). ENSO and Pacific Decadal Variability in Community Climate System Model Version 4. *J. Climate*, *25*, 2622-2651, 10.1175/JCLI-D-11-00301.1.

Gettelman, A., & Morrison, H. (2015). Advanced two-moment bulk microphysics for global models. Part I: Off-line tests and comparison with other schemes. *J. Climate, 28*, 1268–1287, https://doi.org/10.1175/JCLI-D-14-00102.1.

Golaz, J., V.E. Larson, V.E., & Cotton, W.R. (2002). A PDF-Based Model for Boundary Layer Clouds. Part I: Method and Model Description. *J. Atmos. Sci.*, *59*, 3540–3551, https://doi.org/10.1175/1520-0469(2002)059<3540:APBMFB>2.0.CO;2.

570 Goswami, B. N., & Xavier, P.K. (2003). Potential predictability and extended range prediction of
571 Indian summer monsoon breaks. *Geophysical Research Letters*, *30*, doi:10.1029/2003gl017810.
572
573 Hanf, F., & Annamalai, H. (2019): Systematic errors in south Asian monsoon precipitation:
574 process-based diagnostics and sensitivity to entrainment. *J. Climate* (revised)
575
576 Huffman, G.J., et al. (2007). The TRMM Multisatellite Precipitation Analysis (TMPA): Quasi-
577 global, multiyear, combined-sensor precipitation estimates at fine scales. *J. Hydrometeor, 8,* 38–
578 55. doi:10.1175/JHM560.
579
580 Hung, M., Lin, J., Wang, W., Kim, D., Shinoda, T., & Weaver, S.J. (2013). MJO and
581 Convectively Coupled Equatorial Waves Simulated by CMIP5 Climate Models. *J. Climate, 26,*
582 6185–6214, https://doi.org/10.1175/JCLI-D-12-00541.1
583
584 Hurrell, J. W., et al. (2013). The Community Earth System Model: A framework for
585 collaborative research. *Bull. Amer. Meteor. Soc*., *94,* 1339–1360.
586
587 Karmakar, N., & Krishnamurti, T.N. (2019). Characteristics of northward propagating
588 intraseasonal oscillation in the Indian summer monsoon, *Climate Dynamics*, *52*, 1903–1916,
589 https://doi.org/10.1007/s00382-018-4268-2.
590
591 Kay, J. E., et al. (2015). The Community Earth System Model (CESM) Large Ensemble Project:
592 A community resource for studying climate change in the presence of internal climate variability.
593 *Bull. Am. Meteorol. Soc., 96,* 1333–1349, doi:10.1175/BAMS-D-13-00255.1.

Large, W. G., & Yeager, S.G. (2009). The global climatology of an interannually varying air-sea flux data set. *Climate Dyn.*, *33*, 341–364, https://doi.org/10.1007/s00382-008-0441-3.

Liu, X., Ma, P.-L., Wang, H., Tilmes, S., Singh, B., Easter, R.C., Ghan, S.J., & Rasch, P.J. (2016). Description and evaluation of a new four-mode version of the Modal Aerosol Module (MAM4) within version 5.3 of the Community Atmosphere Model. *Geoscientific Model Development*, *9*, 505–522, doi:10.5194/gmd-9-505-2016.

Meehl, G. A., Arblaster, J.M., Lawrence, D., Seth, A., Schneider, E.K., Kirtman, B.P., & Min, D. (2006). Monsoon regimes in the CCSM3. *J. Climate*, **19**, 2482–2495.

Meehl, G.A., Arblaster, J.M., Caron, J., Annamalai, H., Jochum, M., Chakraborty, A., & Murtugudde, R. (2012). Monsoon regimes and processes in CCSM4. Part 1: The Asian-Australian monsoon. *J. Climate*, *25*, 2583—2608, doi: 10.1175/JCLI-D-11-00184.1.

Meehl, G.A., et al. (2019). Effects of model resolution, physics, and coupling on Southern Hemisphere storm tracks in CESM1.3. *Geophys. Res. Lett.*, DOI: 10.1029/2019GL084057.

Neale, R.B., Richter, J.H., & Jochum, M. (2008). The impact of convection on ENSO: From a delayed oscillator to a series of events. *J. Climate*, *21*, 5904–5924, https://doi.org/10.1175/2008JCLI2244.1.

Neena, J.M., Waliser, D., & Jiang, X. (2016). Model performance metrics and process diagnostics for boreal summer intraseasonal variability. *Climate Dynamics*, *48*, 1661–1683, doi:10.1007/s00382-016-3166-8.

Parthasarathy, B., Rupakumar, K., & Munot, A.A. (1991). Evidence of secular variations in Indian monsoon rainfall–circulation relationships. *J. Climate*, *4*, 927–938.

Pillai, P.A., & Annamalai, H. (2012). Moist dynamics of severe monsoons over South Asia: Role of the tropical SST. *J. Atmos. Sci*., *69*, 97-115, doi:10.1175/JAS-D-11-056.1.

Sabeerali, C. T., Dandi, A.R., Dhakate, A., Salunke, K., Mahapatra, S., & Rao, S.A. (2013). Simulation of boreal summer intraseasonal oscillations in the latest CMIP5 coupled GCMs. *J. Geophys. Res: Atmospheres, 118*, 4401–4420, doi:10.1002/jgrd.50403.

Shields, C. A., Kiehl, J.T., & Meehl, G.A. (2016). Future changes in regional precipitation simulated by a half-degree coupled climate model: Sensitivity to horizontal resolution, *J. Adv. Model. Earth Syst.*, *8*, doi:10.1002/2015MS000584.

Sikka, D. R. (1980). Some aspects of the large-scale fluctuations of summer monsoon rainfall over India in relation to fluctuations in the planetary and regional scale circulation parameters. *Proc. Indian Natl. Acad. Sci*., *89*, 179–195.

639 Simpson, I.R., et al. (2019). An evaluation of the large scale atmospheric circulation and its
640 variability in the Community Earth System Model version 2 (CESM2) and other CMIP models,
641 *JAMES*, submitted.
642
643 Sperber, K.R., Annamalai, H., Kang, I.-S., Kitoh, A., Moise, A., Turner, A., Wang, B., & Zhou,
644 T. (2013).The Asian Summer Monsoon: An intercomparison of CMIP5 vs. CMIP3 simulations
645 of the late 20th Century. *Clim. Dyn., 41* (9-10), 2711-2744, doi:10.1007/s00382-012-1607-6.
646
647 Sperber, K.R., & Annamalai, H. (2008). Coupled model simulations of boreal summer
648 intraseasonal (30-50 day) variability, Part I: Systematic errors and caution on use of metrics.
649 *Clim. Dyn.*, *31*, 345-372.
650
651 Suhas, E., Neena, J.M., & Goswami, B.N. (2012). An Indian monsoon intraseasonal oscillations
652 (MISO) index for real time monitoring and forecast verification, *Climate Dynamics*, *40,* 2605-
653 2616, DOI:10.1007/s00382-012-1462-5.
654
655 Turner, A.G., Inness, P.M., & Slingo, J.M. (2005). The role of the basic state in the ENSO-
656 monsoon relationship and implications for predictability. *Quart. J. Roy. Meteor. Soc*., *131*, 781–
657 804.
658
659 Yasunari, T. (1979). Cloudiness fluctuations associated with the Northern Hemisphere summer
660 monsoon. *Journal of the Meteorological Society of Japan. Ser. II*, *57*, 227–242,
661 doi:10.2151/jmsj1965.57.3_227.

Zhang, G., & Mcfarlane, N.A. (1995). Sensitivity of climate simulations to the parameterization of cumulus convection in the Canadian Climate Centre general circulation model. *Atmosphere-Ocean*, *33*, 407–446, doi:10.1080/07055900.1995.9649539.

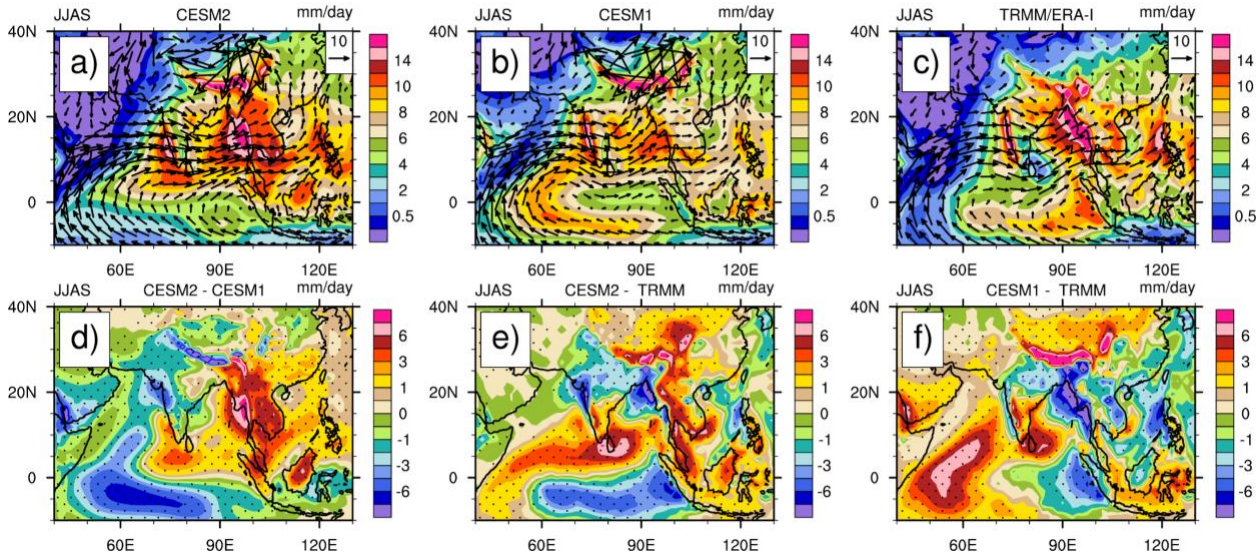

Figure 1: South Asian monsoon precipitation (mm day^{-1}) and 850-hPa wind vectors (m s^{-1}) for JJAS; scaling arrow at upper right (a) CESM2, (b) CESM1, and (c) observations (TRMM/ERA-I); d) precipitation differences, CESM2 minus CESM1; e) same as (d) except for CESM2 minus observations; f) same as (e) except for CESM1 minus observations. An average of 11 ensemble members is shown for the models, model years 1986-2005 chosen to match CESM1 published data. ERA-I data spans 1986-2010 and TRMM data 1998-2013. Stippling in (d)-(f) represents statistically significant differences at the 99% level.

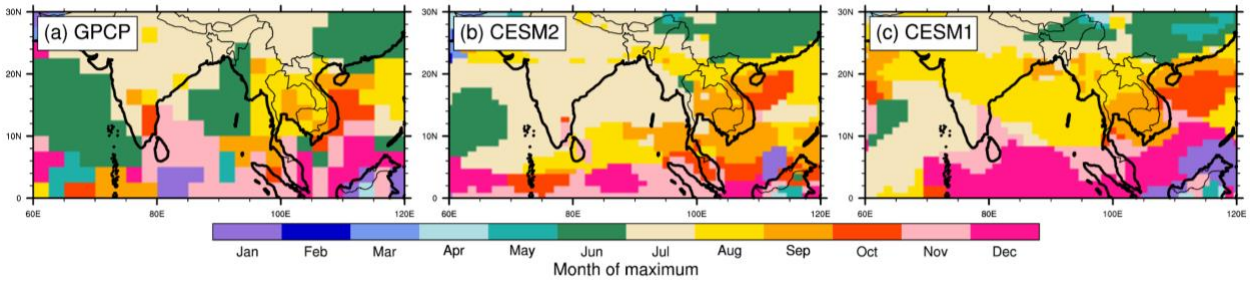

Figure 2: Climatological averaged month of maximum precipitation occurrence from (a) Observed (GPCP), (b) CESM2 and (c) CESM1 over South Asia.

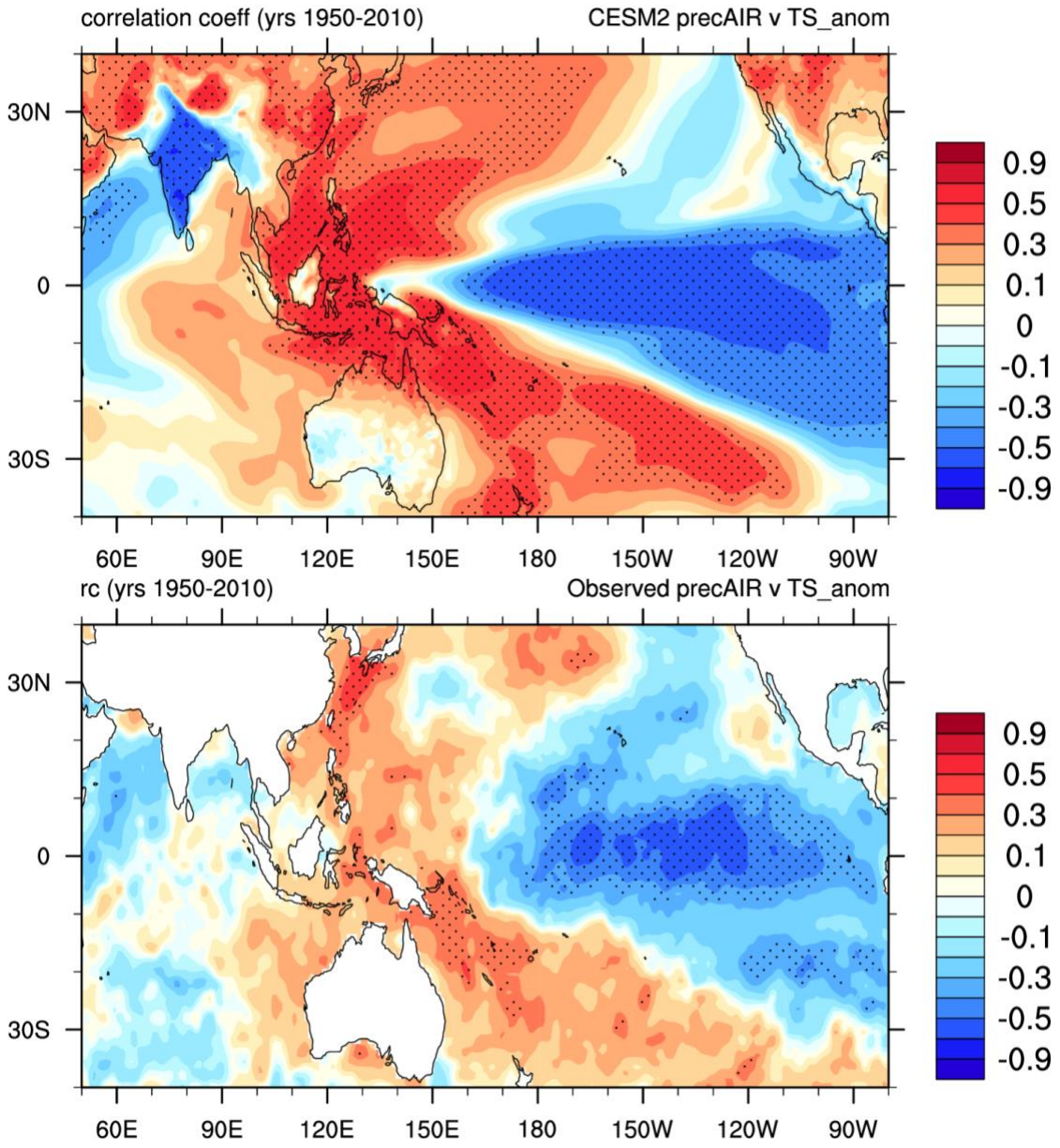

Figure 3: (a) Correlation patterns between seasonal mean (June-September) AIR indices and SST anomalies from CESM2 ensemble mean, and (b) observations. Observations include HadiSST and AIR datasets. Years 1950-2010 are used for both model and observations and stippling indicates statistical significance at the 99% level.

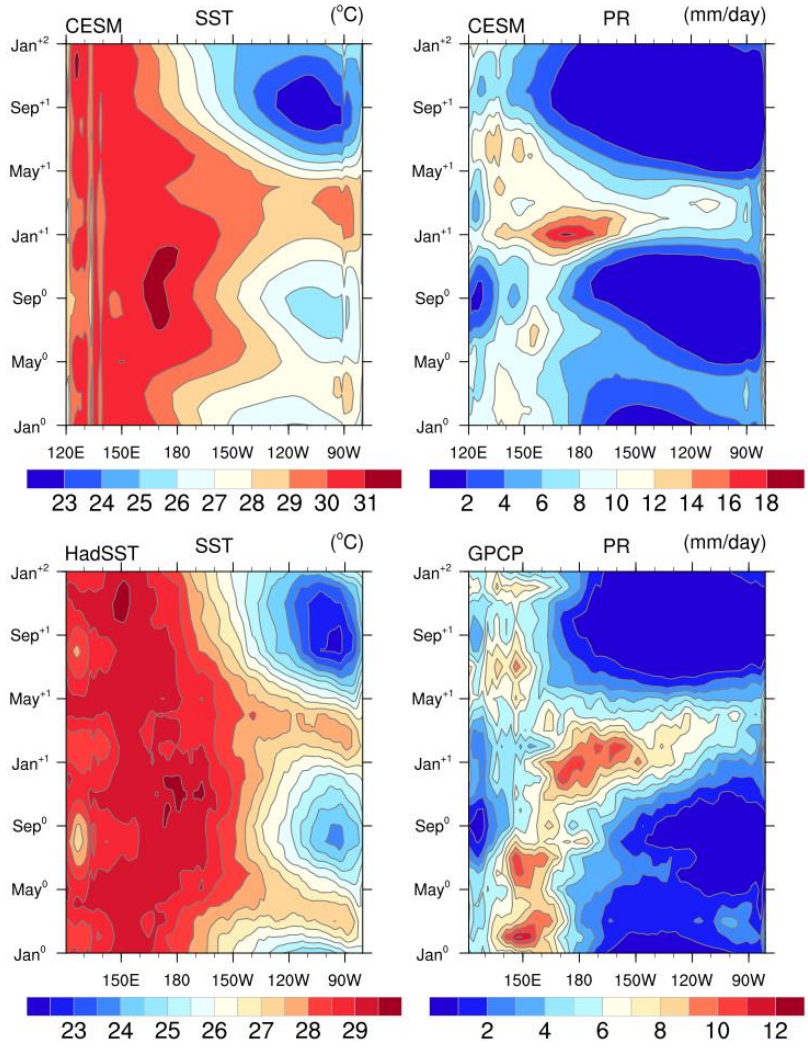

Figure 4: CESM2 El Nino composites from years across all historical ensemble members, a) Nino3.4 total sea surface temperature ($_{o}$C), and b) total precipitation (mm day^{-1}) Latitudes are averaged between 3$_{o}$N and 3$_{o}$S. Composites include all years greater than 1 standard deviation for Nino3.4 SST for all 11 ensemble members; c) same as (a) except for observations; HadiSST years 1870-2018, and d) same as (c) except for observed precipitation composites using GPCP years 1979-2017.

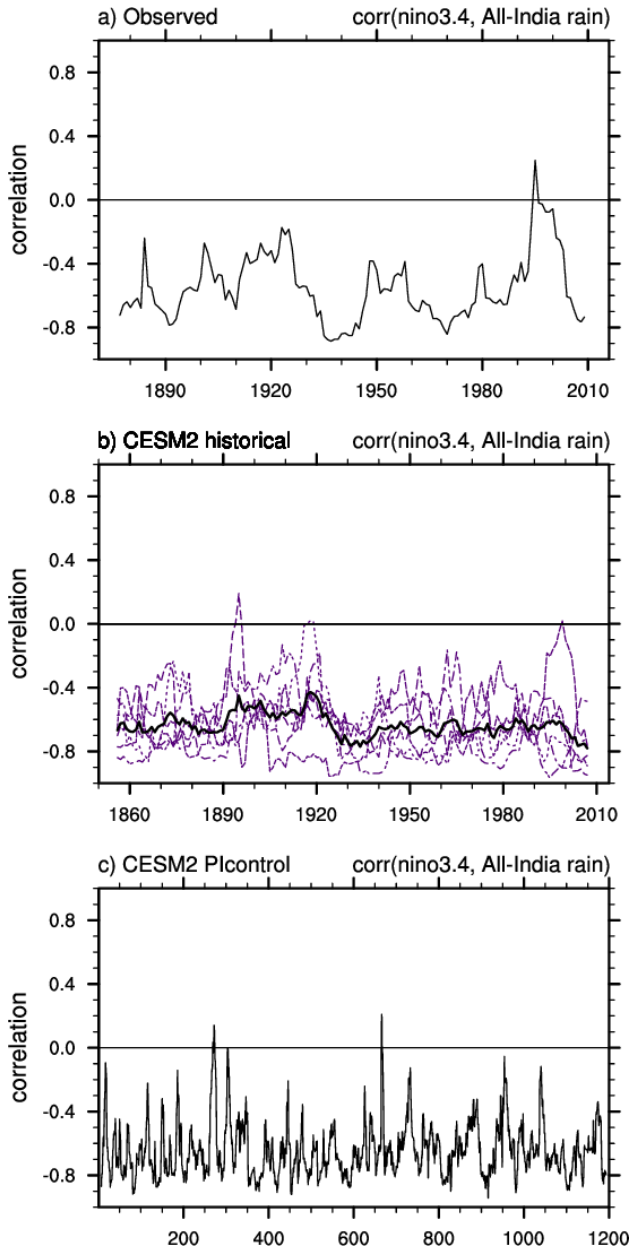

728
729

730 **Figure 5:** Running 13 year correlations between JJAS All-India rainfall (AIR) and Nino3.4

731 SSTs for a) observations, b) individual ensemble members from the CESM2 historical

732 simulation, with the ensemble mean in black; and c) years 1-1200 from the CESM2 pre-

733 industrial control run

734

735
736

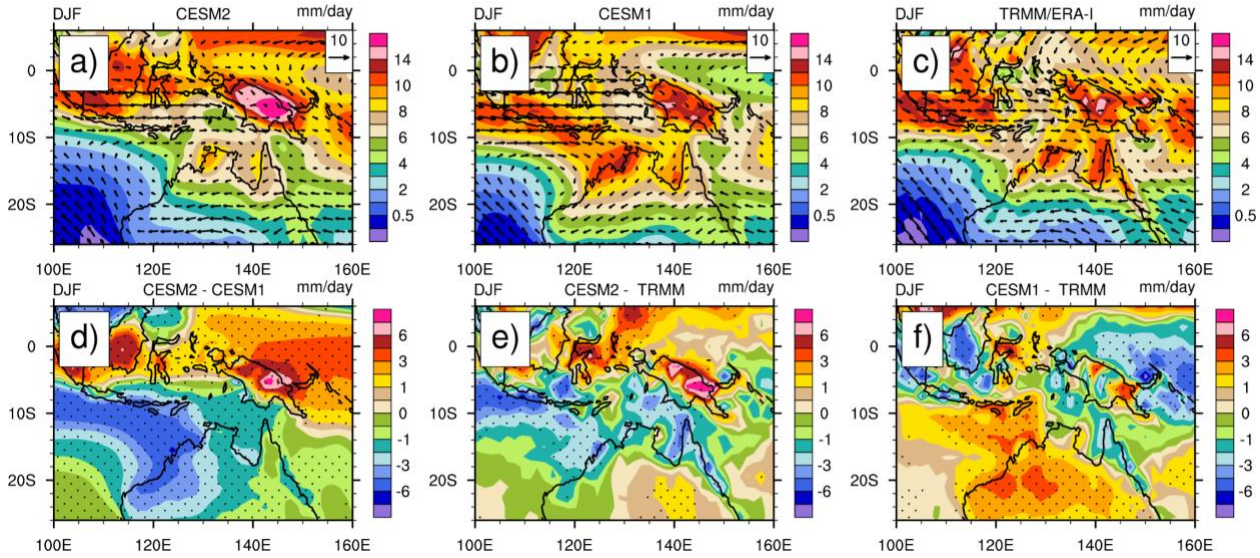

Figure 6: Same as Fig. 1 except for the Australian monsoon, DJF.

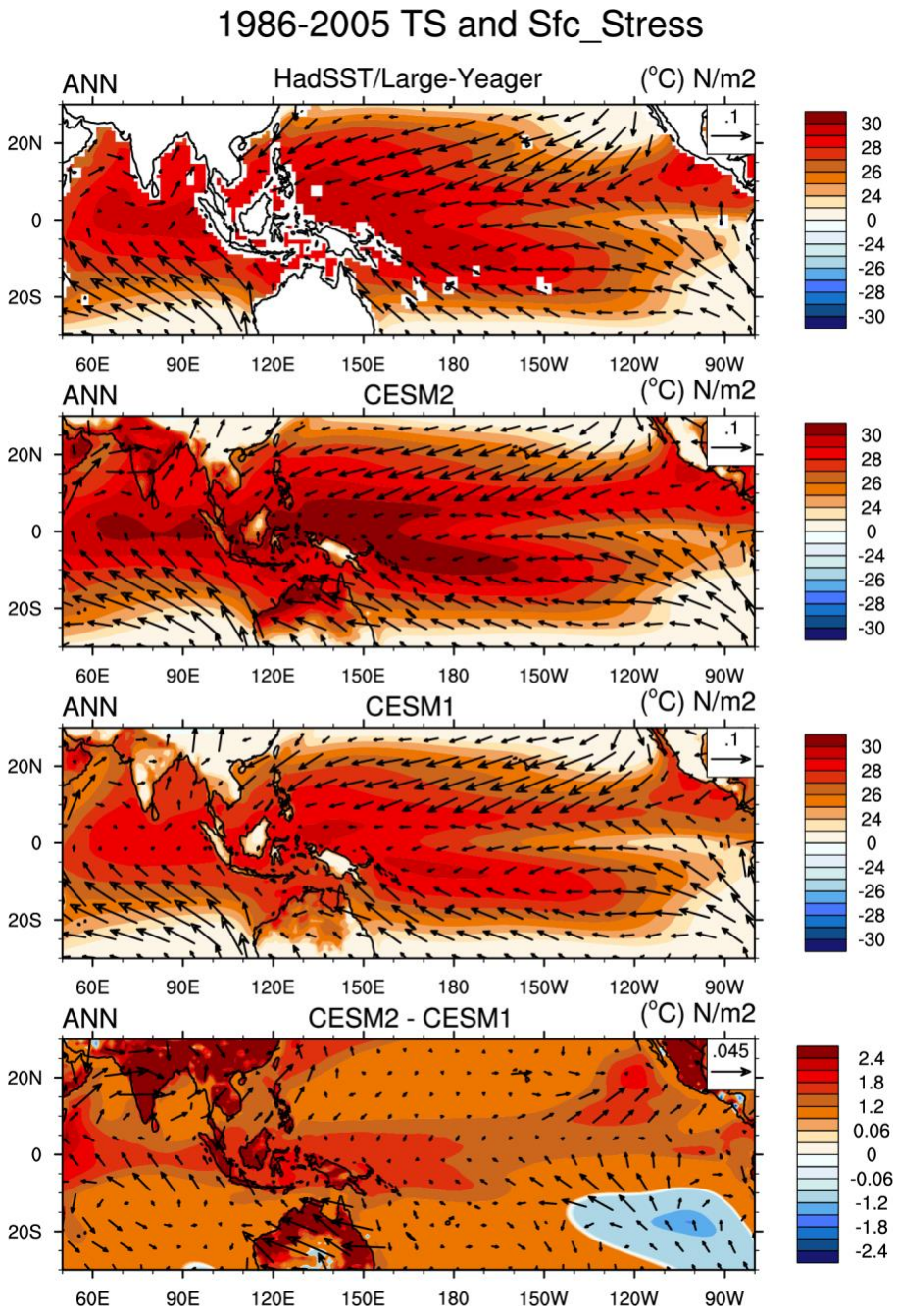

Fig. 7: Annual mean base state surface temperature ($_{o}$C) and wind stress (N m^{-2}, scaling arrow at upper right in each panel) for a) observations (Large and Yeager, 2009; HadSST), b) CESM2, c) CESM1, d) CESM2 minus CESM1.

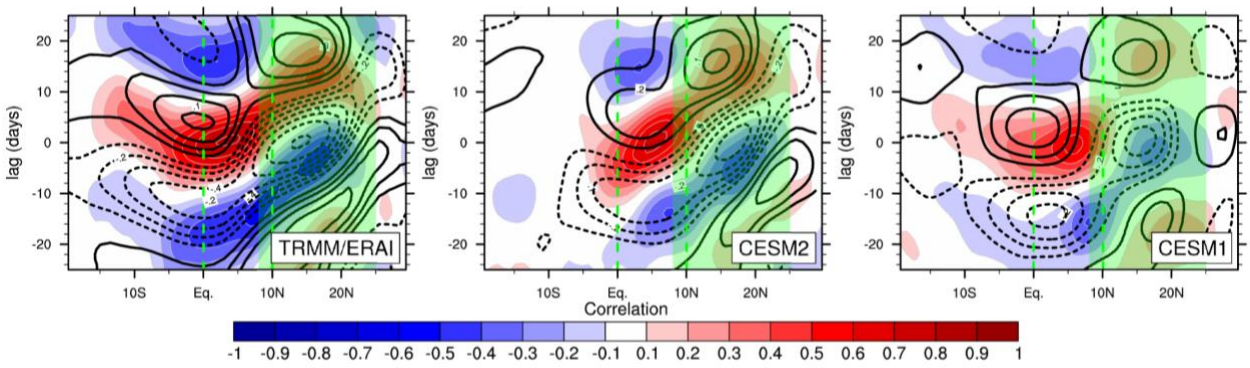

Figure 8: Northward propagation of the Boreal Summer Intraseasonal Oscillation (BSISO) over the south Asian monsoon. Intraseasonal (20-100 day band-pass filtered) lag correlations of precipitation averaged between 0$_o$N and 10$_o$N (green lines), with precipitation (colors) and 850 hPa zonal wind (lines) at latitudes between the Indian Ocean through Eastern India and Bangladesh. Observed (left; 1998-2009), CESM2 (center; 1986-2005) and CESM1 (right; 1986-2005), JJA daily data are averaged between 80$_o$E and 100$_o$E and the Bay of Bengal monsoon region is shown in green shading.

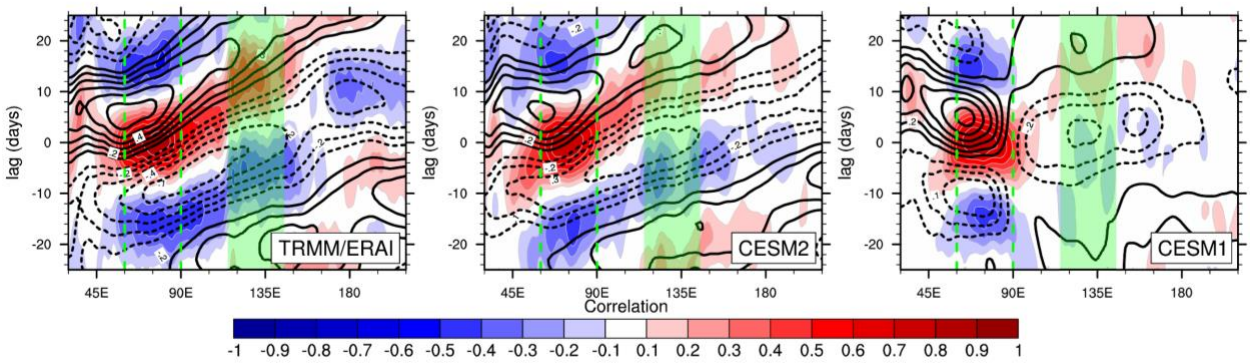

Figure 9: Eastward propagation of the MJO with effects on the Australian monsoon, intraseasonal (20-100 day band-pass filtered) lag correlations of precipitation averaged between 60ₒE and 90ₒE (green dashed lines), with precipitation (colors) and 850 hPa zonal wind (black lines) at longitudes in the Indo-Pacific region. Observed (left; 1998-2009), CESM2 (center; 1986-2005) and CESM1 (right; 1986-2005); DJF daily data are averaged between 15S and 0N and the Australian monsoon region is shown in green shading.

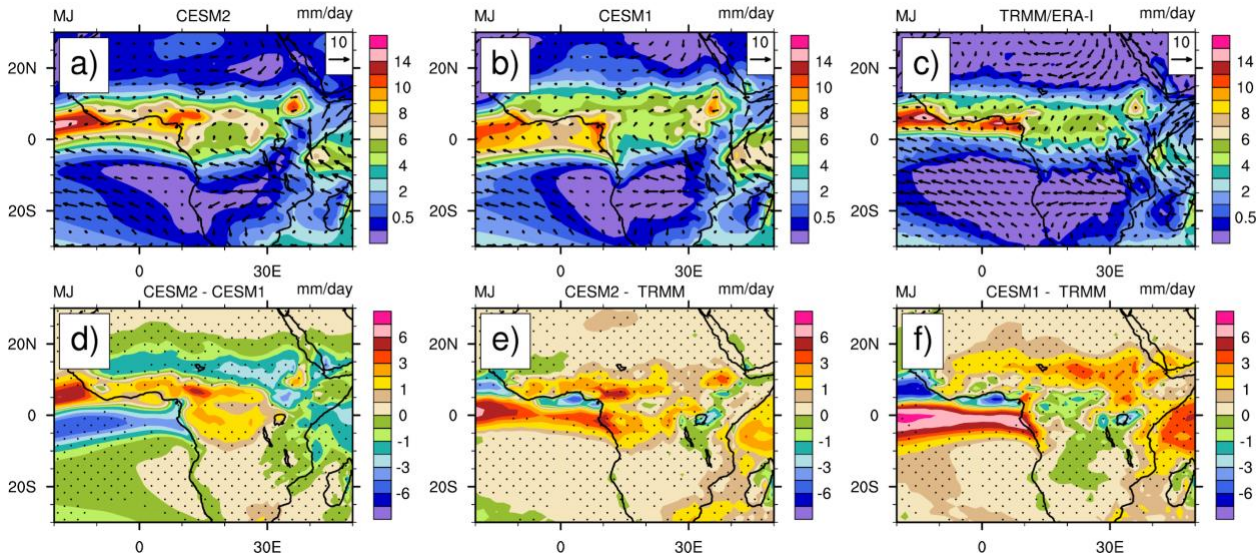

Figure 10: Same as Fig. 1 except for the May-June season in the West African monsoon.

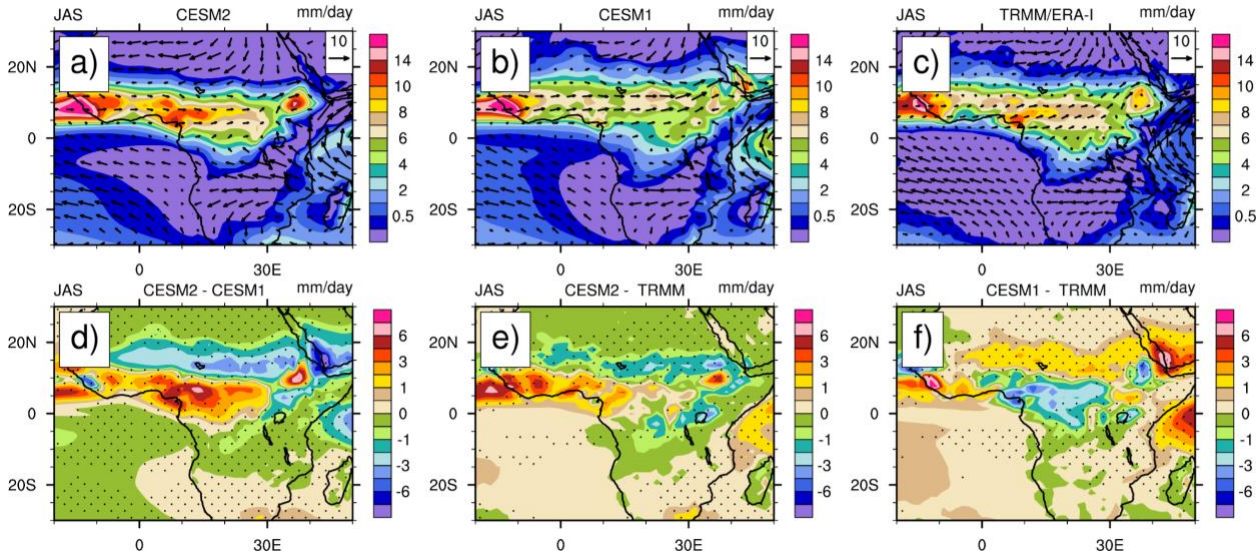

Figure 11: Same as Fig. 1 except for the July-August-September (JAS) season in the West African monsoon.

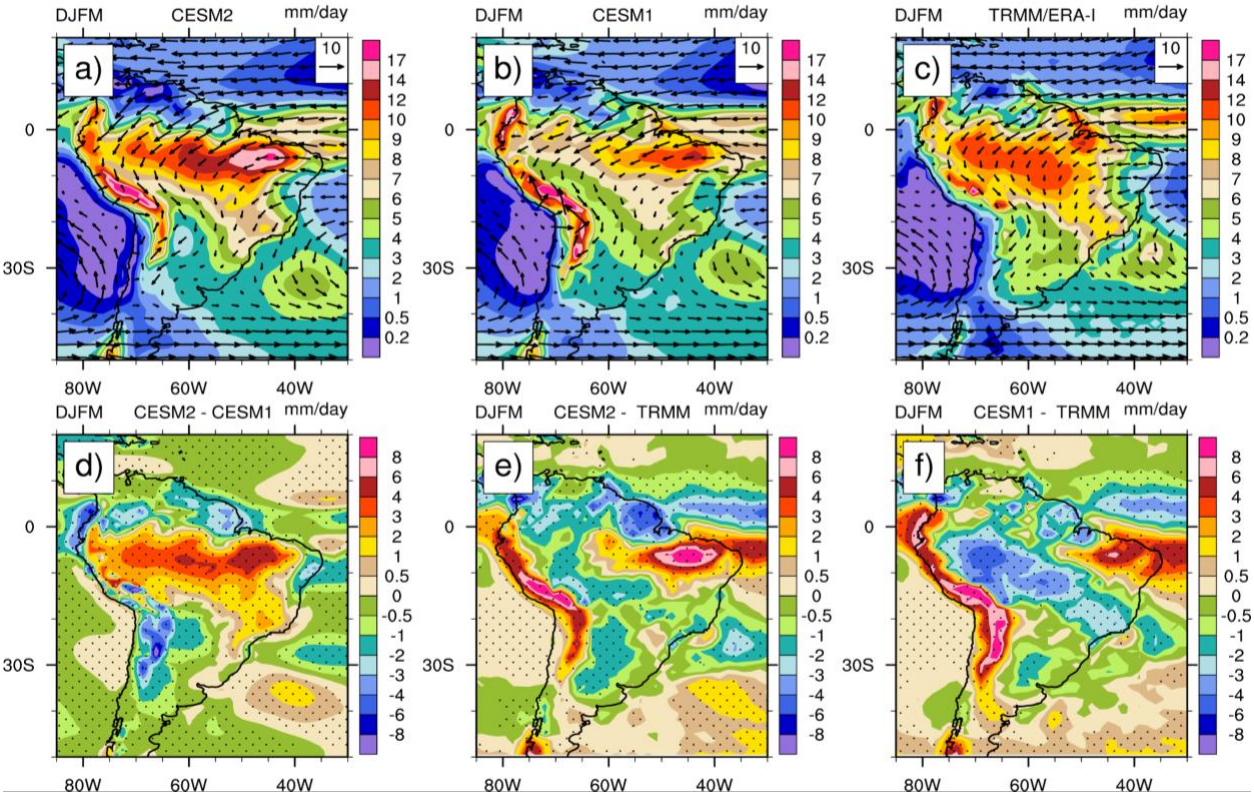

Figure 12: Same as Fig. 1 except for the South American monsoon (DJFM).

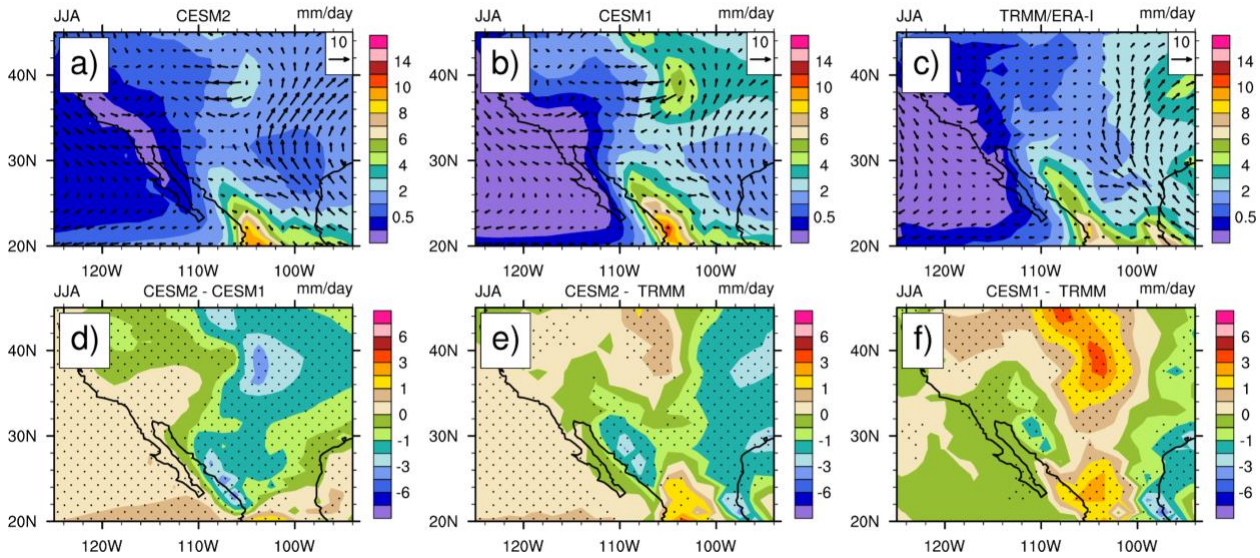

Figure 13: Same as Fig. 1 except for the North American monsoon (JJA).